Preparation and characterization of iron-copper binary oxide and its effective removal of antimony (III) from aqueous solution

Li, Yonchao; Geng, Bing; Hu, Xiaoxian; Ren, Bozhi; Hursthouse, Andrew

Published in:
Water Science & Technology

DOI:
10.2166/wst.2016.219

Published: 01/07/2016

Document Version
Peer reviewed version

Preparation and characterization of iron-copper binary oxide and its effective removal of antimony (III) from aqueous solution

Yongchao Li [a] *, Bing Geng [b], Xiaoxian Hu [a], Bozhi Ren [a] Hursthouse Andrew S [a,c]

[a] School of Civil Engineering, Hunan University of Science and Technology, Xiangtan 411201, China
[b] Institute of Environment and Sustainable Development in Agriculture, Chinese Academy of Agricultural Sciences, Beijing 100081, China
[c] School of Science & Sport, University of the West of Scotland, Paisley, PA1 2BE, Scotland, UK.
* Correspondence should be addressed to Yongchao Li; E-mail: nkliyongchao@163.com

Abstract: A Fe-Cu binary oxide was fabricated through a facile co-precipitation process, and was used to remove Sb(III) from aqueous solution. XRD, SEM, EDX and N_2 adsorption-desorption measurements demonstrated that the Fe-Cu binary oxide consisted of poorly ordered ferrihydrite and CuO, and its specific surface area was higher than both iron oxide and copper oxide. Comparative test indicated that Fe/Cu molar ratio of prepared binary oxide greatly influenced Sb(III) removal and the optimum Fe/Cu molar ratio was about 3/1. Moreover, a maximum adsorption capacity of 209.23 mg Sb(III)/g Fe-Cu binary oxide at pH 5.0 was obtained. The removal of Sb(III) by Fe-Cu binary oxide did follow the Freundlich adsorption isotherm and the pseudo-second-order kinetic in batch study. Sb(III) removal was not sensitive to solution pH. Besides, the release of Fe and Cu ions to water was very small when pH was more than 6.0. XPS analysis confirmed that the Sb(III) adsorbed on the surface was not oxidized to Sb(V).
Key words: adsorption, Fe-Cu binary oxide, Removal mechanism, Sb(III)

INTRODUCTION

Antimony (Sb) is widely used in industrial products including flame retardants, additives in glassware, catalysts for plastics synthesis, and alloys for ammunition. Due to its toxicity and potential carcinogenicity, antimony and its compounds are included as priority pollutants by European Union (1976). To abate health problems associated with Sb, Standardization administration of the People's Republic of China (2006) requires that the maximum contamination level of antimony is lower than 5 μg/L for drinking water. Antimony generally exists in two oxidation states (III and V) in environmental. Sb(V) presents in aerobic condition and Sb(III) persists in anoxic media regularly. Moreover, Sb(III) has a toxicity ten times higher than Sb(V) does (Filella et al. 2007).

In recent years, serious Sb pollution is mostly caused by antimony mining and smelting industries. In the Stampede and Slate Creek watersheds, Sb concentration in stream waters was as high as 720 μg/L, which was associated with historic mining activities within the Kantishna Hills mining district (Ritchiea et al. 2013). Specially, China has the most abundant antimony reserves in the world. In 2007 alone, more than 9.45×10^5 tons of waste water and 6.72×10^5 tons of residue have been produced. Moreover, dissolved antimony in the drainage from Xikuangshan Sb_2S_3 deposit in Hunan Province can be as high as 29.4 mg/L (Zhu et al. 2009). However, it is only treated by precipitation or piped directly into surface water. Not

only is waters and soils around the mine area heavily contaminated but also the health of plants, aquatic species and humans has been damaged in the antimony mine area of China. Since mining and smelting activities discharge massive quantities of waste water, it is thought that significant amounts of Sb(III) persist in deeper water. Therefore, developing effective and economical techniques for Sb(III) removal from aqueous solution is critical.

Major treatment technique for antimony from water includes membrane filtration (Kang et al. 2000), coagulation/flocculation (Guo et al. 2009), and adsorption (Ungureanu et al. 2015) methods. Among these methods, adsorption is one of the most effective choices for the removal of metal ions from water because of its low cost, simplicity, rapidness and high efficiency. Research demonstrates that iron oxides or hydroxides (Guo et al. 2014; Shan et al. 2014; Ungureanu et al. 2015) have higher affinity to Sb(III) than many other adsorbents. Recently, developing composites which have more than one metal oxide has gained considerable attention with obviously synergistic effect. For instances, Fe-Mn binary oxide exhibited much higher Sb(III) removal capacity than both FeOOH and MnO_2 (Xu et al. 2011). In addition, Zn/Fe layered double hydroxide (Lu et al. 2015) adsorbent had preferable removal capacity toward Sb(V). However, studies about Sb(III) adsorption capability exerted by bimetal composites were limited to the Fe-Mn binary oxide.

As a cheap metal oxide, copper oxide provides wide prospects in gas sensors, solar cells and catalyst. Recently, it has been reported that cupric oxide is an effective sorbent for arsenic removal over a wide pH range (Martinson and Reddy, 2009). Furthermore, it has been found that Fe-Cu binary oxide can be a promising adsorbent for As(III) (Zhang et al. 2013). To our best knowledge, although antimony has some similar chemical properties with arsenic, copper based oxide has seldom been studied for Sb(III) removal from aqueous solution.

This manuscript represents the first attempt to study the removal of Sb(III) from aqueous solution by iron based bimetal composites. The main objectives were to (i) prepare a Fe-Cu binary oxide by co-precipitation technique and characterize its structural characteristics; (ii) investigate Sb(III) removal ability of the Fe-Cu binary oxides under various experimental conditions through batch test and optimize the Fe/Cu molar ratio; (iii) illustrate the dominant removal mechanism of Sb(III) by Fe-Cu binary oxide.

EXPERIMENTAL PROCEDURES

Preparation and characterization of Fe-Cu binary oxides

Fe-Cu binary oxides with different Fe/Cu molar ratio were prepared by modified co-precipitation method at the temperature of 23 °C in the laboratory. The preparation steps of Fe-Cu binary oxide with a Fe/Cu molar ratio of 2/1 was as follows. First, a mixed solution containing 2.35 g $FeCl_3 \cdot 6H_2O$ and 0.6 g $CuSO_4$ were prepared. Then 1.25 mol/L NaOH was added drop-wisely into the mixed solution with magnetic stirring. Solution pH was kept at about 9.5 in the reaction process. After continuously stirred for 2 h, the resulting slurry from centrifuge was washed with deionized water, dried at 80 $^{\circ}C$ for 24 h. The final dry materials was ground into fine powder with a mortar and pestle and then used for Sb(III) removal. Fe-Cu binary oxides with a Fe/Cu molar ratio of 1/2, 1/1 and 3/1 were also prepared by altering the amount of $FeCl_3$ or $CuSO_4$ added. Besides copper oxide and iron oxide were

synthesized using similar methods without adding $CuSO_4$ or $FeCl_3$.

Particle morphology and crystallinity were characterized using scanning electron microscopy (SEM, JSM-6380LV, JEOL, Japan) and X-ray diffraction (XRD, D8 Advance, Bruker, Germany). Semi quantitative composition of the surface was examined by means of energy dispersive X-ray spectroscopy (EDX, JSM-6490, JEOL, Japan). Nitrogen adsorption/desorption isotherms were obtained with a NOVA 2200e surface area and pore size analyzer (Quantachrome Instruments, USA) after degassing the samples at 150 °C for 12 h. The specific surface area was calculated using the Brunauer-Emmett-Teller (BET) model, and the pore size distribution was estimated from Barrett-Joyner-Halenda (BJH) method. The chemical state of elements on the surfaces was conducted by X-ray photoelectron spectroscopy (XPS, Kratos Amicus, UK) using monochromatized MgKα X-ray source working at 180 W and 12 kV. Zeta potential of sample at different pH was determined using a JS94H micro-electrophoresis apparatus, which was manufactured by the digital technology equipment of Zhongchen Co., Ltd. Shanghai, China.

Batch experiments

A stock solution of 1000 mg/L Sb(III) was freshly prepared by dissolving 2.738g antimony potassium tartrate ($K(SbO)C_4H_4O_6 \cdot 1/2H_2O$) in 100 mL deionized water. Simulation wastewater of required concentrations were obtained by diluting the Sb(III) stock solution with deionized water. And the Sb(III) solution was prepared as it was used.

The experiments were carried out in 125-mL sealed polypropylene bottles at room temperature (23±1°C). All experiments were performed in duplicate. Comparison test of iron oxide, copper oxide and Fe-Cu binary oxides with different Fe/Cu mole ratio in their abilities to remove Sb(III) was conducted using batch tests. In each test, 0.03 g of iron oxide, copper oxide and Fe-Cu binary oxide was added respectively to 100 mL of 40 mg/L Sb(III) solution after the initial pH was adjusted to 5.0±0.1 with 1.0 mol/L HCl or 1.25 mol/L NaOH. Then these bottles were placed on a rotary shaker at 100 r/min. After 24 h reaction, 3 mL aliquots were taken from the suspension, filtered through 0.45 μm membrane filters and analyzed for Sb remaining in water.

Kinetic experiments were carried out by taking 0.01, 0.02, 0.03 and 0.04 g of Fe-Cu binary oxide with 100 mL of 40 mg/L Sb(III) solution. The initial pH of Sb(III) solution was 5.0±0.1. Samples were taken at the following intervals: 0.5, 1, 2, 4, 6, 10, 12, and 24 h of the reaction, and then filtered to determine the residual Sb concentration in solution.

Sorption isotherms experiments were conducted by taking 0.03 g of Fe-Cu binary oxide with 100 mL of Sb(III) solution varied from 5 to 90 mg/L, respectively. The initial pH of Sb(III) solution was 5.0±0.1. After shaking at 100 r/min for 48 h, the residual Sb concentration in water was analyzed as mentioned before.

To test the effect of solution pH on the removal ability of Fe-Cu binary oxide, the initial pH of Sb(III) solution was pre-adjusted to a desired level from 2.0±0.1 to 12±0.1. Then, 0.03 g of Fe-Cu binary oxide was added into vessel containing 100 mL of 40 mg/L Sb(III) solution, agitated at 100 r/min for 24 h. Then the residual Sb concentration in the solution was determined.

Analytical methods

The pH values of solution were measured using a basic PB-10 meter (Sartorius, Germany). The total Sb and Cu concentrations in solutions were detected by flame atomic absorption spectrophotometer (AA-7001, East & West Analytical Instruments Inc., Beijing). The detection limit of this method was 0.2 mg/L, and the analytical regression coefficient R^2 was greater than 0.997. Total Fe was determined using the 1, 10 phenanthroline spectrometric method (APHA-AWWA-WEF, 1998).

RESULTS AND DISCUSSION

Characterization of iron oxide and copper oxide

XRD pattern of the synthesized iron oxide and copper oxide is shown in Fig. S1a and b. The characteristic peaks of iron oxide approximately at 35°, 55° and 62.5° were features of poorly ordered and amorphous ferrihydrite ($Fe_2O_3 \cdot 2FeOOH \cdot 2.6H_2O$) (Jambor and Dutrizac, 1998; Zhang et al. 2013). The crystalline peaks in copper oxide which appeared at 36.5°, 39°, 49.5° and 62° were in good agreement with those of the standard patterns of CuO (Liu et al. 2015).

N_2 adsorption-desorption isotherms and BJH pore size distribution (inset) of the iron oxide and copper oxide are shown in Fig. S2a and b. The BET surface area and average pore diameter of iron oxide were calculated to be 82.39 m^2/g and 3.893 nm, respectively. The BET surface area and average pore diameter of copper oxide were determined to be 28.13 m^2/g and 3.796 nm, respectively.

Characterization of Fe-Cu binary oxide

Fig. 1 shows XRD patterns of the prepared binary oxide with theoretical Fe/Cu molar ratios of 1/2, 1/1, 2/1 and 3/1. It can been seen that, the Fe-Cu binary oxide components were complex, both ferrihydrite characteristic peak at 35°, 55° and 62.5°, and CuO characteristic peaks at 36.5°, 39°, 49.5° and 62° occurred. Moreover, Fe-Cu binary oxides existed mainly in amorphous form.

Fig. 2 illustrates the SEM images of Fe-Cu binary oxide with different Fe/Cu atom ratio. It was shown that most of binary oxides were not of uniform size, certain particles reached the nanometer grade, and some were greater than 10 μm. Moreover, they were composed of many aggregated small particles, which resulted in a rough surface. In addition, the structure of binary oxide with Fe/Cu molar ratio of 1/2 (Fig. 2a) was relatively flocculent loose, However, with the increase of iron oxide constituents, the binary oxide with Fe/Cu molar ratio of 3/1 (Fig. 2d) was typically massive and compact.

The EDX spectrum of sample was conducted and the result is shown in Fig. S3, It revealed that Fe, Cu, and O were the main elemental composition of products, which agreed well with the XRD results. As there is oxygen in the atmosphere, the obtained value for O was inexact. Therefore, the average atomic ratios of elements Fe and Cu are summarized in Table S1. It can be seen that experimental values of Fe/Cu molar ratio agreed well with

the theoretical value, which indicated that the preparation method for the binary oxides had a good reliability.

Fig. 3 illustrates N_2 adsorption-desorption isotherms and pore size distribution analysis of the binary oxides with Fe/Cu molar ratio of 1/1 and 3/1. The isotherms of two samples exhibited the characteristics of types IV isotherms with a H3 type hysteresis loop, which was typically observed for materials with slit-shaped mesopores of packing particles (Passe-Coutrin et al. 2008). The binary oxide with Fe/Cu molar ratio of 1/1 had a BET surface area of 119.17 m^2/g, and the average pore diameter was about 3.397 nm. The BET surface area and pore diameter of binary oxide with the Fe/Cu molar ratio of 3/1 was 238.79 m^2/g and 2.165 nm. Obviously, the surface area of Fe-Cu binary oxide with Fe/Cu molar ratio of 3/1 increased significantly compared to binary oxide with the Fe/Cu molar ratio of 1/1, iron oxide and copper oxide.

Additionally, the analysis of zeta potential in Fig. S4 indicated that the point of zero charge of Fe-Cu binary oxide in presence of 0.01 M NaCl was about pH 7.7.

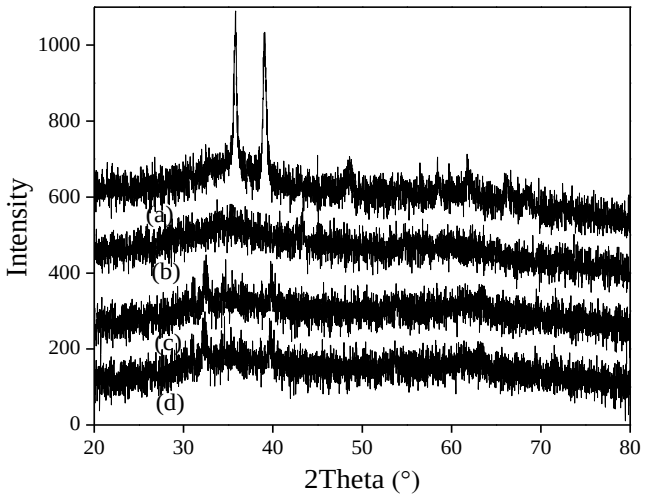

Fig. 1 XRD patterns of prepared binary oxides with Fe/Cu molar ratio of (a) 1/2, (b) 1/1, (c) 2/1 and (d) 3/1.

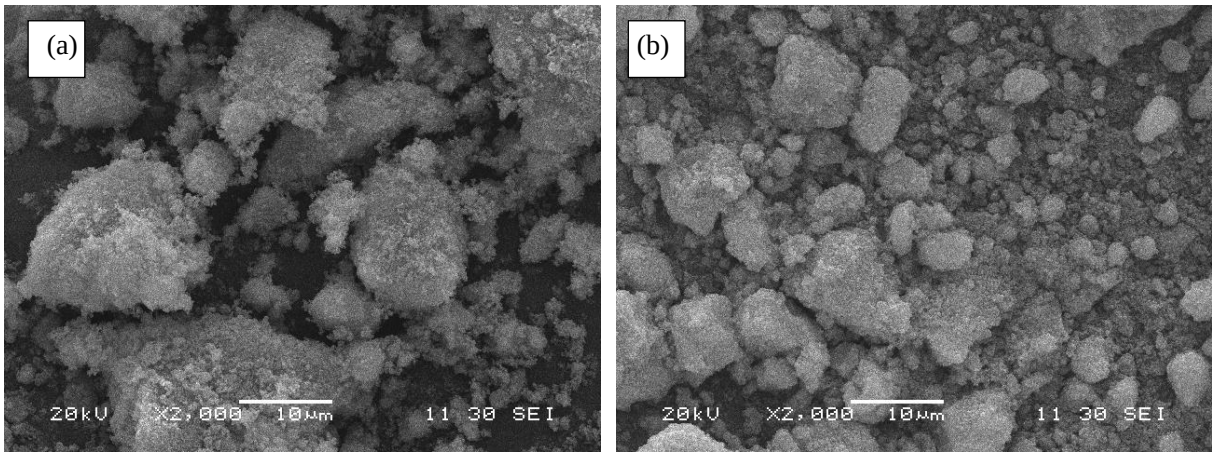

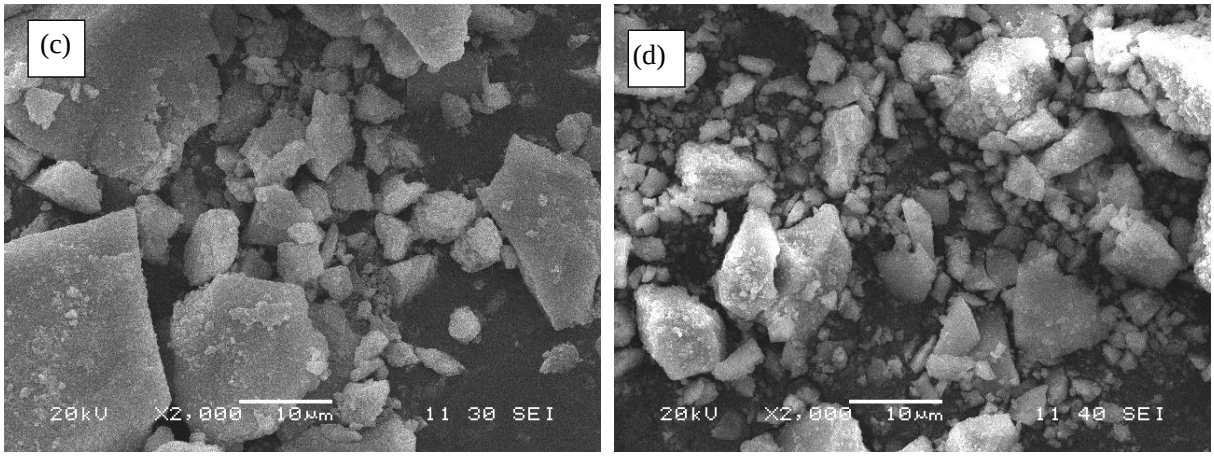

Fig. 2 SEM images of Fe-Cu binary oxide with Fe/Cu molar ratio of (a) 1/2, (b) 1/1, (c) 2/1 and (d) 3/1.

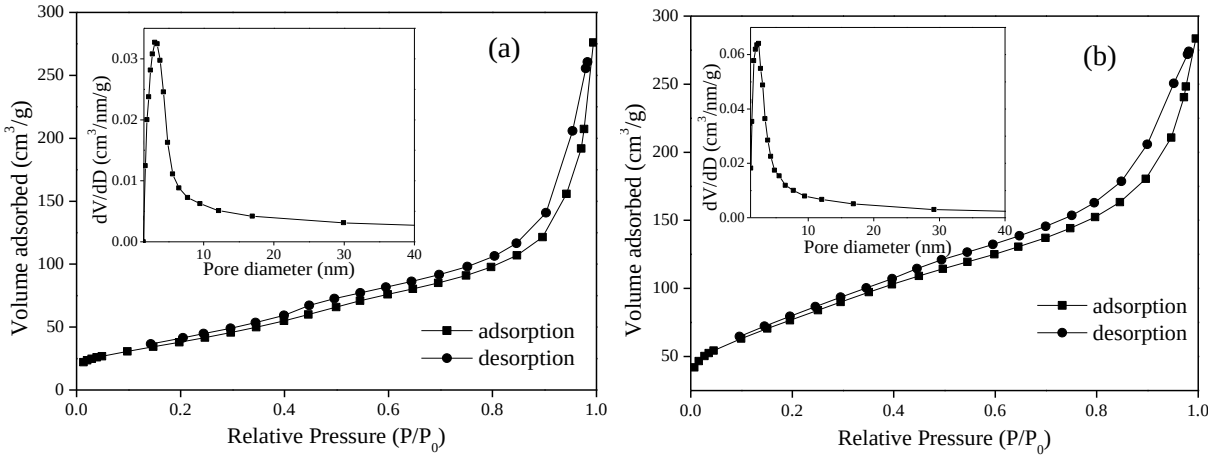

Fig. 3 N_2 adsorption-desorption isotherm and pore size distribution curve of (a) Fe-Cu binary oxide with the Fe/Cu molar ratio of 1/1 and (b) Fe-Cu binary oxide with the Fe/Cu molar ratio of 3/1.

Comparison of Sb(III) removal ability between metal oxide and bimetal oxide

After 24 h reaction, 56.29% and 22.5% of 40 mg/L Sb(III) was removed separately by 0.3 g/L of iron oxide and pure copper oxide. At the same reaction condition, the Sb(III) removal rate of binary oxide with Fe/Cu molar ratio of 3/1, 2/1, 1/1, 1/2 was 81.30%, 76.42%, 67.32% and 64.85% correspondingly. It was obvious that with incorporation of copper into iron oxide, Sb(III) removal ability of the Fe-Cu binary oxide increased obviously. Moreover, the adsorption of Sb(III) on binary oxide with the Fe/Cu molar ratio of 3/1 reached a maximum and then dropped down as copper oxide constituent continued to increase. It was known that the BET surface area of iron oxide, copper oxide, and binary oxide with Fe/Cu of 1/1, 3/1 was 82.39, 28.13, 119.17, 238.79 m^2/g respectively. So, the high surface area for Fe-Cu binary oxide might be an important reason in improving Sb(III) sorption capacity. Meanwhile, since the adsorption ability of pure copper oxide was lower than iron oxide, excess copper oxide constituents in composites was not perfect. Above all the Fe/Cu molar ratio was a key factor influencing the sorption capacity of the Fe-Cu binary oxide, and the

optimum Fe/Cu molar ratio was about 3/1, which was then used in the following experiments.

Kinetics of Sb(III) adsorption on Fe-Cu binary oxide surface

The experiments for kinetic study were conducted by equilibrating the 100 mL of 40 mg/L Sb(III) solution with a series of binary oxide with Fe/Cu molar ratio of 3/1 for different time intervals. Fig. 4 shows the amount of Sb(III) adsorbed onto Fe-Cu binary oxide at a contact time. It was observed that the removal capacity of Sb(III) increased rapidly before 4 h contact time, and then slowed down as equilibrium was approached at about 24 h. The high initial removal rate may be attributed to the existence of large number of adsorption sites on the surface of fine particles. As the sites filled up gradually, the intra-particle diffusion process dominated in the adsorption of Sb, and the removal became slow.

Pseudo-first-order kinetic and pseudo-second-order kinetic model equation have long been widely applied in the sorption system. The linear forms of the pseudo-first-order and pseudo-second-order equations are expressed as Eq. (1) and Eq. (2):

$$\ln(q_e - q_t) = \ln q_e - k_1 t \qquad (1)$$

$$\frac{t}{q_t} = \frac{1}{k_2 q_e^{\,2}} + \frac{t}{q_e} \qquad (2)$$

where q_e (mg/g) and q_t (mg/g) were the amount of adsorbed Sb(III) at equilibrium and at any time t (h), k_1 (1/h) and k_2 (g/(mg·h)) are the rate constant for pseudo-first-order and pseudo-second-order sorption, respectively. The fitting of the pseudo-first-order and pseudo-second-order kinetic model for the adsorption of Sb(III) by Fe-Cu binary oxide are shown in Fig. 4. The corresponding parameters are included in Table S2. The R^2 for the pseudo-first-order model indicated that the model was inapplicable to fit the kinetic data. However, the R^2 values for pseudo-second-order kinetic model were in range of 0.9729-0.9934, and the calculated q_e values were in highly accordance with the experimental q_e values. So it can be concluded that the pseudo-second-order kinetic model was able to describe the adsorption of Sb(III) onto Fe-Cu binary binary oxide, and the adsorption process was mainly controlled by the chemisorption process (Ho and McKay 2000). It was known that there were a substantial amount of chemically active Fe-OOH on ferrihydrite surface (Jambor and Dutrizac 1998), and Xu et al. (2011) had also reported that Fe-OOH groups was able to interact with the Sb.

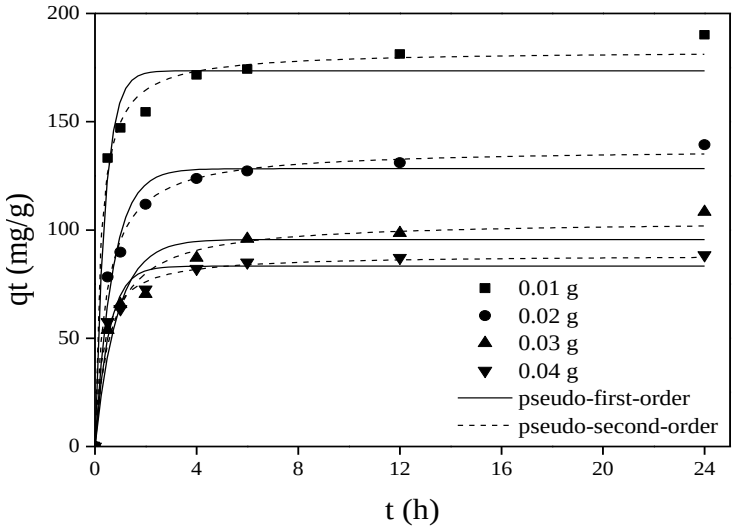

Fig. 4 Effect of the contact time on adsorption of Sb(III) onto the Fe-Cu binary oxide. Initial Sb(III) concentration: 40 mg/L, pH: 5.0±0.1, 23±1°C.

Adsorption Isotherms

To describe the equilibrium adsorption behavior of Sb(III), Langmuir and Freundlich isotherm models were used to analyze the equilibrium data. The Langmuir sorption isotherm is valid for monolayer adsorption onto a surface containing a finite number of identical sites. The Freundlich isotherm model allows for several kinds of sorption sites on the solid and properly represents the sorption data at low and intermediate concentrations on heterogeneous surfaces. The equations of Langmuir and Freundlich isotherm model can be expressed by Eq. (3) and Eq. (4):

$$q_e = \frac{K_L q_m C_e}{1 + K_L C_e} \qquad (3)$$

$$q_e = K_f C_e^{1/n} \qquad (4)$$

where q_e is Sb amount adsorbed onto Fe-Cu binary oxide at equilibrium (mg/g); C_e is equilibrium concentration of Sb in the aqueous solution (mg/L); ‘‘q_m’’ is the maximum sorption capacity (mg/g); K_L is the Langmuir sorption constant (L/mg) which is related to the energy of adsorption. K_f ($mg^{(1-1/n)}L^{1/n}/g$) and n are the Freundlich constants which are indicators of adsorption capacity and adsorption intensity.

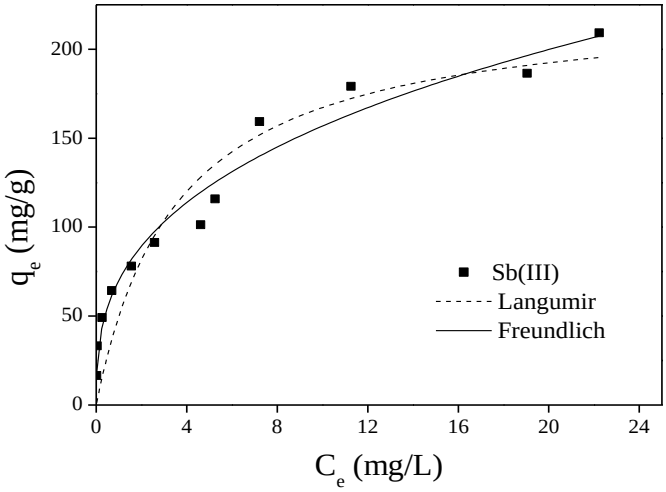

Fig. 5 Variation of the adsorbed Sb on the Fe-Cu binary oxide at equilibrium. Initial Sb(III) concentration: 5-90 mg/L, sorbent dose: 0.3 g/L, pH: 5.0±0.1, 23±1°C.

Fig. 5 highlights the experimental data as well as the isotherm models for the adsorption of Sb(III) on Fe-Cu binary oxide. The calculated parameters of Langmuir and Freundlich isotherm models are presented in Table S3. The higher correlation coefficients (R^2) indicated that Freundlich model fitted the adsorption data better than the Langmuir model over the entire range of adsorptive concentration studied. The fractional value of 1/n ($0<1/n<1$) obtained clearly corresponded to a heterogeneous surface. It was because that the simultaneous presence of ferrihydrite and CuO in the binary oxide led to a heterogeneous surface of the Fe-Cu binary oxide with different sorption energies.

As being indicated by the direct experimental data in Fig. 5, the maximal removal capacity of Fe-Cu binary oxide toward Sb(III) was 209.23 mg/g at the initial Sb(III) concentration of 90 mg/L. The comparison of the maximum adsorption capacities of various adsorbents for Sb(III) are shown in Table 1. It was found that Fe-Cu binary oxide in this study exhibited higher adsorption capacity than many other adsorbents, which made it a possible efficient adsorbent for Sb(III) removal from aqueous solutions.

Table 1 Comparison of adsorption capacity for Sb(III) from aqueous solution reported in literature

Adsorbent	Concentration range (mg/L)	pH	Q_{max} (mg/g)	T (K)	References
Goethite (α-FeOOH)	1.13-33.83	9.0	53.45	293	(Guo et al. 2014)
Green bean husk	2.5-100	4.0	20.14	298	(Iqbal et al. 2013)
Nano-zero valent iron stabilized by polyvinyl alcohol	0-20	7.0	6.99	298	(Zhao et al. 2014)
Carbon nanofibers decorated with ZrO_2	10-500	7.0	79.83	298	(Luo et al. 2015)
Fe-Mn binary oxide	23-225	3.0	214.28	293	(Xu et al. 2011)
Fe(III)-loaded saponified orange	—	10.5	136	303	(Biswas et al. 2009)
α-Fe_2O_3 coated Fe_3O_4	1-20	4.1	36.7	298	(Shan et al. 2014)
Mercapto-functionalized hybrid sorbent	100-300	5.0	108.8	298	(Fan et al. 2016)
Fe-Cu binary oxide	5-85	5.0	209.23	296	This study

Effect of the solution pH on Sb(III) adsorption and metal leaching of Fe-Cu binary oxide

The effect of pH on Sb(III) adsorption onto the Fe-Cu binary oxide is shown in Fig. 6a. It can be seen that 87.96% and 81.11% of Sb(III) was removed by 0.03 g Fe-Cu binary oxide when the initial solution pH was 2.0 and 4.0, separately. The Sb(III) removal rate was kept to about 85% in the pH range 6.0-10.0. However, Sb(III) adsorption suddenly decreased by 25.6% when pH increased from 10.0 to 12.0. Moreover, in all experiments solution pH rose by 0.2-0.5 after 24 h reaction. It was known that solution pH was one of the more important factors affecting adsorption process. In present study, Sb(III) existed as $(SbO)C_4H_4O_6^-$ coordination anions. The positive charge of Fe-Cu binary oxide surface gradually dropped with increase of pH, as illustrated in Fig. S4, and the electrostatic attraction between the negatively charged antimony tartrate ion and the more negative charged surface of Fe-Cu binary oxide became weaker, thereby would result in the decrease of Sb(III) adsorption. However, this was not reflected by the drops of Sb(III) removal until solution pH increased to 12.0. This phenomenon suggested that the pH-dependent electrostatic attraction did not control the adsorption process onto Fe-Cu binary oxide. Adsorption was likely to be based on chemical adsorption which was also supported by the kinetics analysis.

Fig. 6b demonstrates the concentrations of dissolved Fe and Cu in water after reaction under different pHs. It was shown that the leaching of Fe and Cu was serious under acid condition. When the pH was more than 6.0, the Fe and Cu concentration was below 0.3 mg/L and 1 mg/L respectively, which is the limit of drinking water standard of China (SAC 2006). Therefore, the prepared Fe-Cu binary oxide can be used to safely treat actual antimony mine drainage, most of which was neutral or weakly alkaline in China (Zhu et al. 2009).

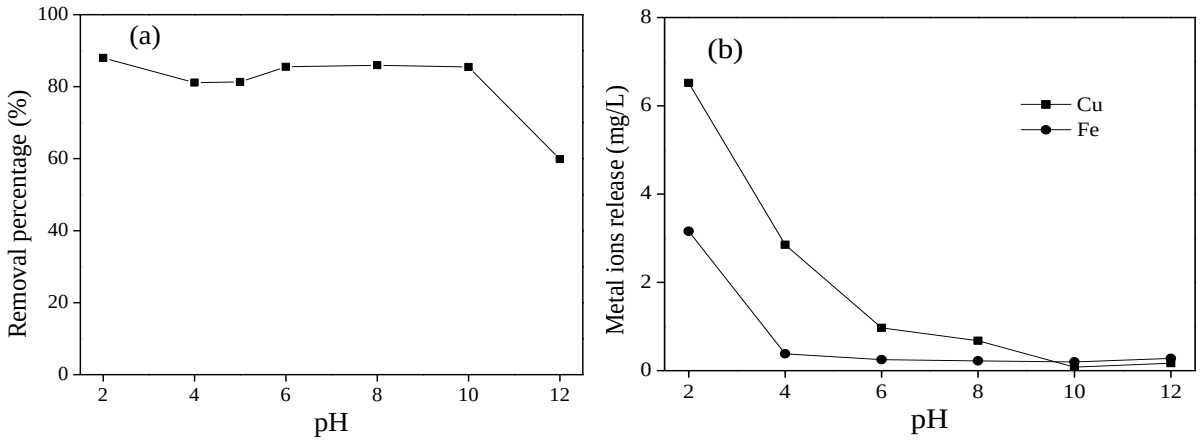

Fig. 6 (a) Effect of solution pH on Sb(III) removal, (b) Release of Fe and Cu to solution after reaction. Initial Sb(III) concentration: 40 mg/L, sorbent dose: 0.3 g/L, pH: 5.0±0.1, 23±1°C.

Further discussion of removal mechanism

After reaction, the Fe-Cu binary oxide was recovered from the reaction solution, then SEM and EDX was employed to characterize the product morphological properties and

elementary composition. The results are shown in Fig. S5. Compared with the freshly prepared Fe-Cu binary oxide which was sharp-edged block (Fig. 2d), the morphology of the Fe-Cu binary oxide surface was markedly changed after reaction, and some flocculus appeared on the surface of material (Fig. S5a). EDX spectra (Fig. S5b) revealed that Fe and Cu were the primary elements, but the Fe/Cu molar ratio was changed to 3.26 resulting from the leaching of binary oxide. Besides, 15.85 *weight*% Sb was observed on the Fe-Cu binary oxide surface after reaction.

To further obtain the oxidation state of elements on the surface, XPS spectra of the Fe-Cu binary oxide after reaction was analyzed. As shown in Fig. 7a, Sb 3d peaks as well as Fe 2p, Cu 2p and O 1d peaks appeared, which proved once again that the reaction product of Sb precipitated on the surface of Fe-Cu binary oxide. Detailed XPS surveys on the region of Fe 2p and Cu 2p are presented in Fig. 7b and c. The particles exhibited Fe $2p_{3/2}$ and $2p_{1/2}$ binding energies of about 710.95 and 724.5 eV, which were close to the binding energies of Fe(III) species (Xu et al. 2011). The photo-electron peaks for Cu $2p_{1/2}$ and Cu $2p_{3/2}$ were present at binding energy 954 eV and 933.74 eV, indicating that Cu(II) was the predominant copper species on the surface (Biesinger et al. 2010). Due to the overlapping of O 1s and Sb 3d photo-electron peaks regularly, deconvolution of the XPS spectra of Sb 3d+O 1s was performed and plotted in Fig. 7d. Although the binding energy of Sb(III) and Sb(V) in XPS spectra was reported to be too close to allow individual quantification, the Sb $3d_{3/2}$ binding energy of Sb(III) adsorbed sample was lower than the 540.1 binding energy for Sb(V) oxide (Izquierdo et al. 1989). The peaks of Sb $3d_{5/2}$ and Sb $3d_{3/2}$ at 529.7 eV and 539.79 eV in this study can be assigned to Sb(III). Therefore, XPS measurement demonstrated that the chemical valence state of Fe(III) and Cu(II) during the sorption process did not change, and the oxidation of Sb(III) did not occur. Consequently, it was proposed that the ferrihydrite and CuO groups were the main adsorption sites available for Sb. These results are similar to the found by Xu et al. (2011) in the case of FeOOH. However, Guo et al. (2014) found that the majority of Sb(III) adsorbed onto hydrous ferric oxide was oxidized into Sb(V) probably due to the involvement of O_2 in the long duration of sample preservation.

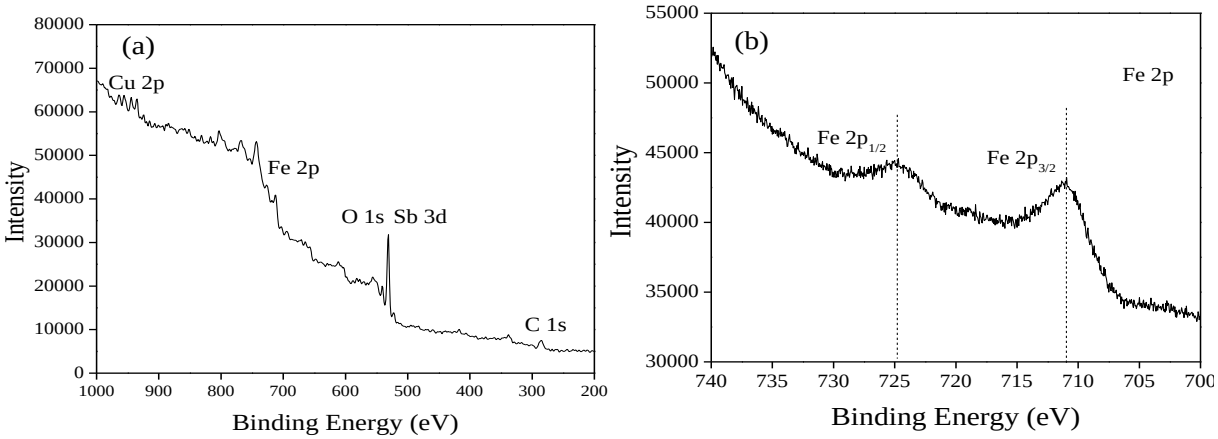

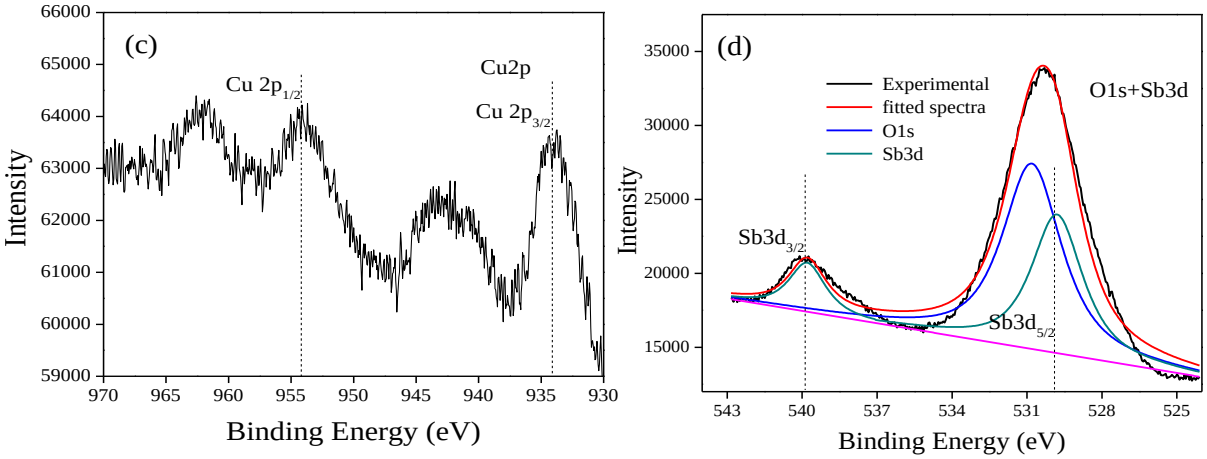

Fig. 7 (a) XPS wide survey for Fe-Cu binary oxide after reaction with Sb(III). High-resolution XPS survey for (b) Fe 2p, (c) Cu 2p and (d) O 1s+Sb 3d of Fe-Cu binary oxide after reaction.

CONCLUSIONS

This study demonstrated for the first time that Sb(III) can be effectively adsorbed by Fe-Cu binary oxide from the aqueous solution. Batch adsorption experiments were carried out under various conditions, such as the initial Sb(III) concentration, material dose, contact time, and solution pH. The result indicated that Sb(III) removal ability of prepared binary oxide with Fe/Cu molar ratio of 3/1 was best. The pseudo-second-order kinetic provided the best correlation for the adsorption process, indicating the process was controlled by the chemisorption process. The adsorption isotherms of Sb(III) onto Fe-Cu binary oxide could be described well by the Freundlich isotherm better than the Langmuir isotherm. Moreover, Sb(III) adsorption reaction was not sensitive to the solution pH. The Fe and Cu release to aqueous solution was below the limit of drinking water standard of China when the pH was more than 6.0. In addition, the XPS spectra confirmed that Sb(III) adsorbed onto the Fe-Cu binary oxide was not oxidized into Sb(V). In conclusion, the Fe-Cu binary oxide was a promising adsorbent for Sb(III) removal from contaminated water as a result of its excellent removal performance, simple synthesis process and no secondary pollution. Continuous treatment of practical antimony mine drainage using Fe-Cu binary oxides packed fixed bed reactor will be investigated further.

ACKNOWLEDGMENTS

This work was supported by the National Natural Science Foundation of China (No. 51504094).

REFERENCES

APHA-AWWA-WEF 1998. Standard methods for examination of water and wastewater, 20th edition, American public health association, Washington, DC.

Biesinger, M.C., Laua, L.W.M., Gerson, A.R., Smart, R.S.C. 2010. Resolving surface chemical states in XPS analysis of first row transition metals, oxides and hydroxides: Sc, Ti, V, Cu and Zn. Appl. Surf. Sci. 257 (3), 887–898.

Biswas, B.K., Inoue, J.I., Kawakita, H., Ohto, K., Inoue, K. 2009. Effective removal and recovery of antimony using metal-loaded saponified orange waste. J. Hazard. Mater.172 (2-3), 721–728.

Council of the European Communities 1976. Council Directive 76/464/EEC of 4 May 1976 on pollution caused by certain dangerous substances discharged into the aquatic environment of the community, Official Journal L 129, 23–29.

Fan, H.T., Sun, W., Jing, B., Wang, Q.J., Li, D.W., Huang, C.C., et al. 2016. Adsorption of antimony(III) from aqueous solution by mercapto-functionalized silica-supported organic-inorganic hybrid sorbent: Mechanism insights. Chem. Eng. J. 286, 128–138.

Filella, M., Belzile, N., Lett, M.C. 2007. Antimony in the environment: A review focused on natural waters. III. Microbiota relevant interactions. Earth-Sci. Rev. 80, 195–217.

Guo, X.J., Wu, Z.J., He, M.C. 2009. Removal of antimony (V) and antimony (III) from drinking water by coagulation-flocculation-sedimentation (CFS). Water Res. 43 (17), 4327–4335.

Guo, X.J., Wu, Z.J., He, M.C., Meng, X.G., Jin, X., Qiu, N., et al. 2014. Adsorption of antimony onto iron oxyhydroxides: Adsorption behavior and surface structure. J. Hazard. Mater. 276 (9), 339–345.

Ho, Y.S., McKay, G., 2000. The kinetics of sorption of divalent metal ions onto sphagnum moss peat. Water Res. 34 (3), 735–742.

Iqbal, M., Saeed, A., Edyvean, R.G.J. 2013. Bioremoval of antimony(III) from contaminated water using several plant wastes: Optimization of batch and dynamic flow conditions for sorption by green bean husk (Vigna radiata). Chem. Eng. J. 225 (3), 192–201.

Izquierdo, R., Sacher, E., Yelon, A. 1989. X-ray photoelectron spectra of antimony oxides. Appl. Surf. Sci. 40 (1-2), 175–177.

Jambor, J.L., Dutrizac, J.E. 1998. Occurrence and constitution of natural and synthetic ferrihydrite, a widespread iron oxyhydroxide. Chem. Rev. 98 (7), 2549–2585

Kang, M., Kawasaki, M., Tamada, S., Kamei, T., Magara, Y. 2000. Effect of pH on the removal of arsenic and antimony using reverse osmosis membranes. Desalination, 131(1-3), 293-298.

Liu, X., Cui, S.S., Sun, Z.J., Du. P.W. 2015. Copper oxide nanomaterials synthesized from simple copper salts as active catalysts for electrocatalytic water oxidation. Electrochimica Acta 160, 202–208.

Lu, H.T., Zhu, Z.L., Zhang, H., Zhu, J.Y., Qiu, Y.L. 2015. Simultaneous removal of arsenate and antimonate in simulated and practical water samples by adsorption onto Zn/Fe layered double hydroxide. Chem. Eng. J. 276, 365–375.

Luo, J.M., Luo, X.B., Crittenden, J., Qu, J.H., Bai, Y.H., Peng, Y., et al. 2015. Removal of antimonite (Sb(III)) and antimonate (Sb(V)) from aqueous solution using carbon nanofibers that are decorated with zirconium oxide (ZrO_2). Environ. Sci. Technol. 49 (18), 11115−11124.

Martinson, C.A., Reddy, K.J. 2009. Adsorption of arsenic(III) and arsenic(V) by cupric oxide nanoparticles. J. Colloid Interf. Sci. 336 (2), 406–411.

Passe-Coutrin, N., Altenor, S., Cossement, D., Jean-Marius, C., Gaspard, S. 2008. Comparison of parameters calculated from the BET and Freundlich isotherms obtained by nitrogen adsorption on activated carbons: A new method for calculating the specific surface area. Micropor. Mesopor. Mat. 111 (1), 517–522.

Ritchie, V.J., IIgen, A.G., Mueller, S.H., Trainor, T.P., Goldfarb, R.J. 2013. Mobility and chemical fate of antimony and arsenic in historic mining environments of the Kantishna Hills district, Denali National Park and Preserve, Alaska. Chem. Geol. 335 (1), 172–188.

Shan, C., Ma, Z.Y., Tong, M.P. 2014. Efficient removal of trace antimony(III) through adsorption by hematite modified magnetic nanoparticles. J. Hazard. Mater. 268 (3), 229–236.

Standardization administration of the People's Republic of China (SAC) 2006. Standards for drinking water quality (GB5749-2006), Beijing.

Ungureanu, G., Santos, S., Boaventura, R., Botelho, C. 2015. Arsenic and antimony in water and wastewater: Overview of removal techniques with special reference to latest advances in adsorption. J. Environ. Manage. 151, 326–342.

Xu, W., Wang, H.J., Liu, R.P., Zhao, X., Qu, J.H. 2011. The mechanism of antimony(III) removal and its reactions on the surfaces of Fe-Mn Binary Oxide. J. Colloid Interf. Sci. 363 (1), 320–326.

Zhao, X.Q., Dou, X.M., Mohan, D., Pittman, C.U., OK, Y.S., Jin, X., 2014. Antimonate and antimonite adsorption by a polyvinyl alcohol-stabilized granular adsorbent containing nanoscale zero-valent iron. Chem. Eng. J. 247(7), 250–257.

Zhang, G.S., Ren, Z.M., Zhang, X.W., Chen. J. 2013. Nanostructured iron(III)-copper(II) binary oxide: A novel adsorbent for enhanced arsenic removal from aqueous solutions. Water Res. 47 (12), 4022–4031.

Zhu, J., Wu, F.C., Deng, Q.J., Shao, S.X., Mo, C.L., Pan, X.L., et al. 2009. Environmental characteristics of water near the Xikuangshan antimony mine, Hunan Province. Acta Scientiae Circumstantiae, 29 (3), 655–661.

Supplementary Material：

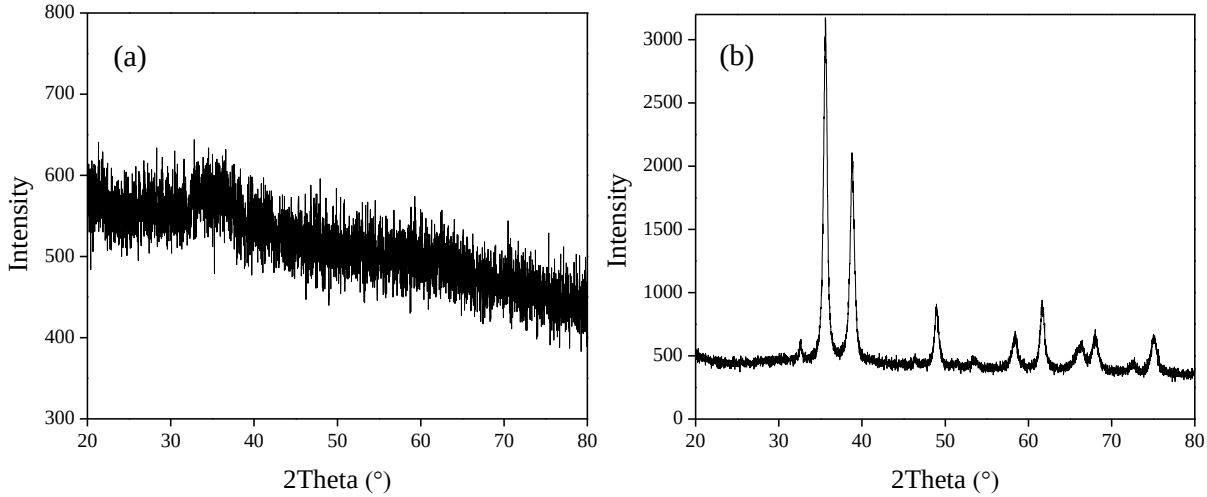

Fig. S1 XRD patterns of prepared (a) iron oxide and (b) copper oxide.

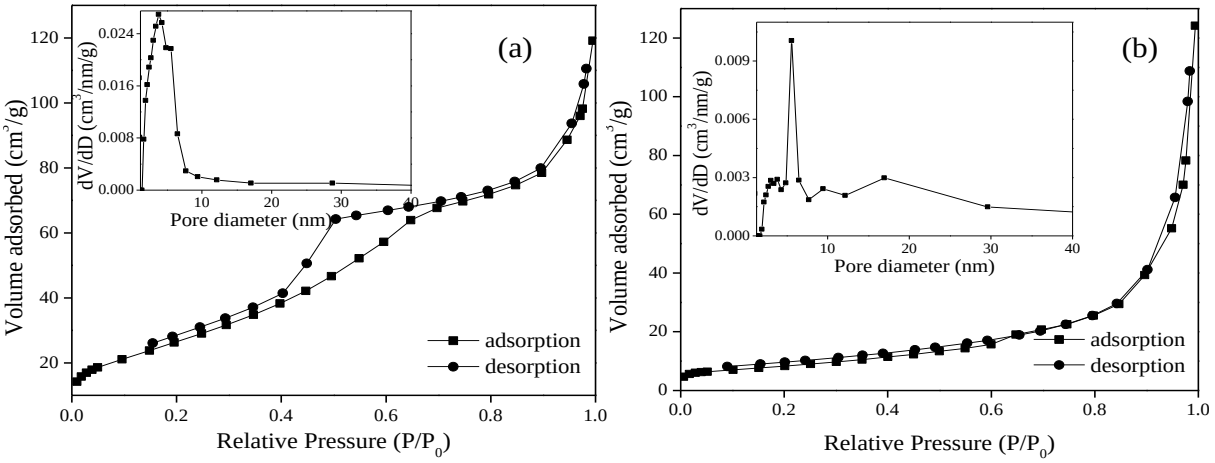

Fig. S2 N_2 adsorption-desorption isotherm and pore size distribution curve of (a) iron oxide and (b) copper oxide.

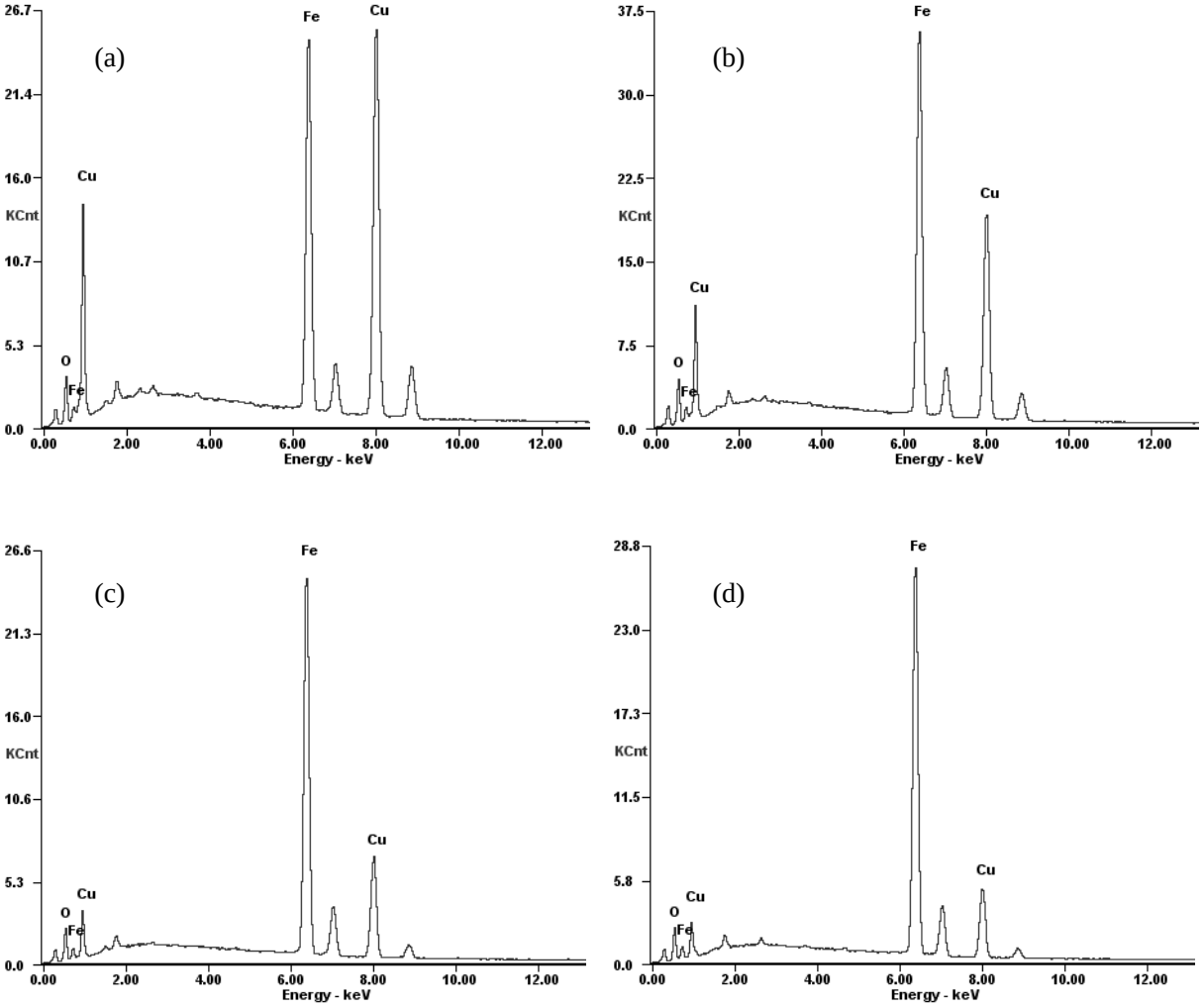

Fig. S3 EDX patterns of Fe-Cu binary oxide with Fe/Cu atom ratio of (a) 1/2, (b) 1/1, (c) 2/1 and (d) 3/1.

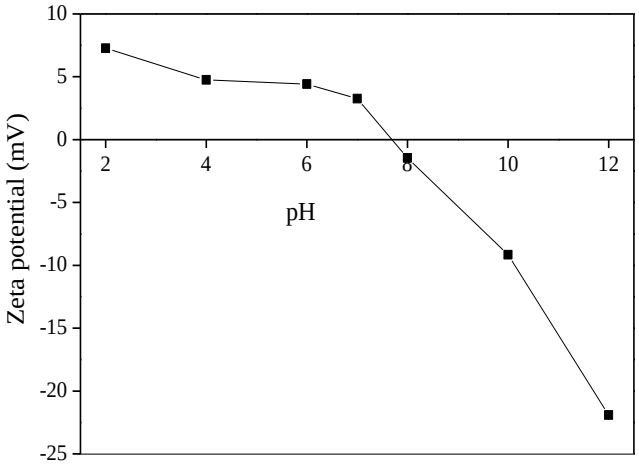

Fig. S4 Zeta potentials of binary oxide with the Fe/Cu molar ratio of 3/1 over a wide pH range.

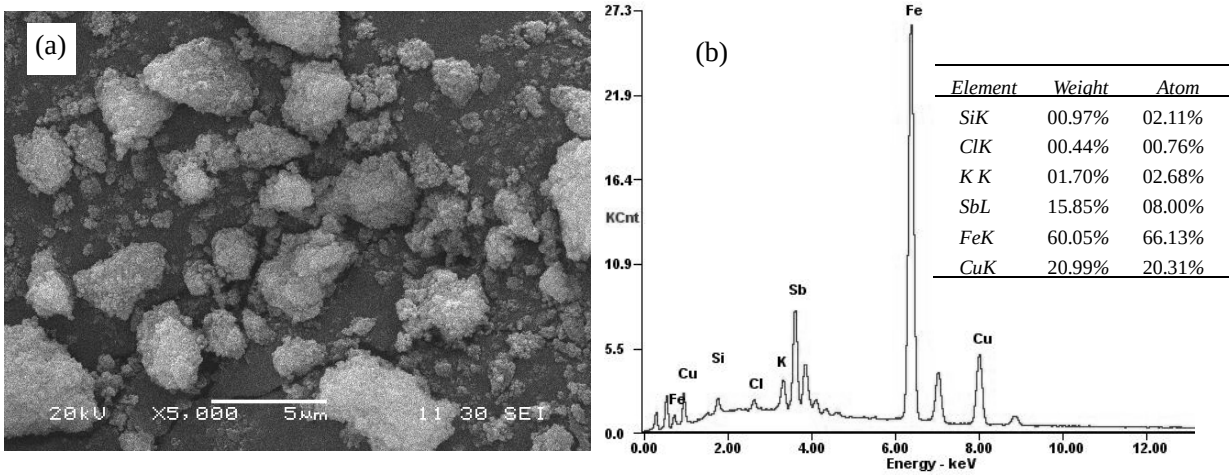

Fig. S5 (a) SEM image and (b) EDX spectra of Fe-Cu binary oxide after reaction. Initial Sb(III) concentration: 40 mg/L, sorbent dose: 0.3 g/L, pH: 5.0±0.1, 23±1°C.

Table S1 Elemental composition of the prepared Fe-Cu binary oxides obtained from EDX spectrum

	Fe/Cu molar ratio (theoretical value)	Fe/Cu molar ratio (experimental value)	Fe *Atom*% (EDX)	Cu *Atom*% (EDX)
binary oxide	1/2	1/1.95	33.88%	66.12%
binary oxide	1/1	1/1	50.11%	49.89%
binary oxide	2/1	2.08/1	67.53%	32.47%
binary oxide	3/1	3.07/1	75.45%	24.55%

Table S2 Kinetic constants obtained from pseudo-first-order and pseudo-second-order model.

			pseudo-first-order			pseudo-second-order		
Binary oxide dose (g/L)	Sb(III) (mg/L)	$q_{e,exp}$ (mg/g)	K_1 (1/h)	$q_{e,cal}$ (mg/g)	R^2	K_2 (g/(mg·h))	$q_{e,cal}$ (mg/g)	R^2
0.1	40	190.09	2.53	173.52	0.9600	0.025	182.83	0.9892
0.2	40	139.33	1.44	128.30	0.9636	0.016	137.61	0.9934
0.3	40	108.41	1.15	95.61	0.9144	0.016	104.44	0.9729
0.4	40	88.42	1.83	83.29	0.9578	0.035	88.52	0.9918

Table S3 Langmuir and Freundlich isotherm parameters of Sb(III) adsorption to Fe-Cu binary oxide

Langmuir			Freundlich		
q_{max}(mg/g)	K_L(L/mg)	R^2	1/n	K_F ($mg^{(1-1/n)}L^{1/n}/g$)	R^2
226.55	0.282	0.8884	0.35	70.08	0.9673